

Core-scale characterisation of flow in tight Arabian formations

Lateef T. Akanji · Ghasem G. Nasr ·
Mohamed Bageri

Received: 26 September 2012 / Accepted: 7 May 2013 / Published online: 24 June 2013
© The Author(s) 2013. This article is published with open access at Springerlink.com

Abstract Production from tight reservoirs usually requires enhancement due to problems associated with very low permeability. The collection of the fundamental knowledge database needed to fully understand the key mechanisms affecting flow behaviour in tight formation is still sparse. In this paper, we applied a new technique of measuring flow properties in porous media to characterise flow behaviour in core samples of tight carbonate formations. A high-pressure automatic mercury injection apparatus was used to directly estimate basic routine data of tight core samples. The result of this experimental study showed that entry capillary pressure required for the mercury to intrude the pore-space, is strongly dependent on pore-size distribution; typically high (≈ 13.79 MPa) for average pore-size of about 70 nm and low (< 0.07 MPa) for average pore-size of 1 μm in the carbonate core samples. Moreover, the permeability of the samples is higher for the core samples obtained vertically through the parent rock.

Keywords Tight formation · Entry capillary pressure · Pore intrusion · Pore-size · Permeability

Introduction

Tight formations are considered to be reservoirs with an absolute permeability of generally less than 10 mD and can

range down to micro-Darcy range, (μD or 10^{-6} Darcy) in many situations. These reservoirs could potentially serve as media for the storage of commercial accumulation of hydrocarbon. However, production and ultimate recovery are usually uneconomical due to a number of factors which include: poor reservoir quality, unfavourable initial saturation condition, formation damage caused by drilling and completion operations, hydraulic or acid fracturing, kill or work-over treatments and other production-related problems (Bahrami et al. 2011).

Many tight reservoirs are extremely complex producing oil or gas from multiple layers with low permeabilities that often require enhancement by natural fractures. Despite the marginal economics and low productivity from these reservoirs, the soaring demands for energy has necessitated a devotion of technologies to optimise recovery. Description of the pore geometry of reservoirs plays a major role in understanding the degree of pore inter-connectivity, pore-shapes and sizes, capillary trapping potentials and flow behaviour (e.g. Bliefnick and Kaldi 1996; Melas and Friedman 1992; Vavra et al. 1992).

Mercury injection method is a widely used technique for the evaluation of capillary pressure and pore-size and pore-size distribution of porous formation (e.g. Purcell 1949; Brooks and Corey 1981; Katz and Thompson 1987; Pittman 1992). Other petrophysical characteristics such as porosity and irreducible water saturation are determined using mercury porosimetry. These petrophysical properties determine the shape, slopes and plateau of the capillary pressure curve. Although, the differences between air/mercury and brine/hydrocarbon systems do not allow mercury injection method to reproduce reservoir-specific conditions; it provides a very accurate analogue when calibrated to measured and calculated values of reservoir fluid properties (Vavra et al. 1992).

L. T. Akanji (✉) · G. G. Nasr
Petroleum and Gas Engineering Division, School of Computing
Science and Engineering, University of Salford, Manchester, UK
e-mail: l.t.akanji@salford.ac.uk

M. Bageri
Department of Petroleum and Natural Gas Engineering,
King Saud University, Riyadh, Saudi Arabia

Mercury injection capillary pressure (MICP) measurements may also be integrated with seismic and micro-structural data to provide a robust basis for interpretation of the reservoir sealing capacity, storage and trapping potentials and stability/strength of individual strata. Analysis of the MICP curve is, therefore, important for various phases of reservoir production, especially secondary and tertiary recovery from tight formation. These data may also be evaluated in conjunction with additional special and routine core data to accurately assess the reservoir and/or sealing potential.

In order to optimise production from tight reservoirs, adequate pore-to-macro-scale characterisation is required to establish the influence of pore-scale geometries on flow properties at the macro-scale (e.g. Akanji and Matthai 2010). A lot has been done on estimation of both air and absolute permeability of basic rock properties from MICP measurements (e.g. Klinkenberg 1941; Archie 1950; Brooks and Corey 1981; Katz and Thompson 1981; Thompson et al. 1987; Dastidar et al. 2007; Walls and Amaefule 1985; Khan et al. 2011); however, technologies required for the acquisition of accurate rock–fluid interaction data necessary to understand flow behaviour in tight formations with permeability in the micro-Darcy (μD) range are currently being researched (e.g. Swanson 1966; Huet et al. 2005; Comisky et al. 2007). Furthermore, the effect of capillarity on flow property variation in a vertically and horizontally obtained tight core samples is still not well understood.

The aim of this work is therefore to investigate the interrelation between pore capillary data and flow parameters of tight core samples obtained vertically and horizontally from parent rock. An advanced state-of-the-art automatic pore intrusion (AutoPore IV) apparatus capable of injecting non-wetting phase (mercury) in user-defined, step-like pressure increments up to 414 MPa (60,000 psi) was utilised. Each core sample was evacuated and cleaned/dried prior to the running of the experiment. An innovative laboratory approach was used to control injection direction thereby allowing basic petrophysical parameters to be accurately derived and flow behaviour determined.

Capillary pressure determination using high-pressure mercury injection

High-pressure automatic mercury injection apparatus was used in the characterisation of the tight core samples. The volume of injected mercury (S_{Hg}) at each pressure increment is automatically recorded until the maximum analytical pressure, or 100 % pore-volume mercury saturation is achieved. Pressure is then plotted against incremental mercury saturation (S_{Hg}) readings to generate the drainage curve.

When two immiscible fluids co-exist, the rock–fluid interaction can be defined by the capillary pressure measured across the interface. Mercury is used as the injection fluid since it is non-wetting and non-reactive with most solid surfaces. Furthermore, it has a contact angle of about 140° for most solids and therefore requires the application of pressure before intruding the pore-spaces. Utilising this approach, air is then assumed to be the wetting phase while mercury is the non-wetting phase (Melrose et al. 1994); capillary pressure is therefore defined as:

$$P_c = P_{\text{nw}} - P_w, \quad (1)$$

where P_w and P_{nw} are the wetting (air) and non-wetting (mercury) capillary pressure, respectively.

The wetting-phase is retained within the porous medium by surface adhesion forces holding the fluid as a film completely covering the rock surfaces and by capillary forces separating it and the liquid.

Estimation of porosity and permeability from mercury injection method

The porosity ϕ from the mercury injection method is estimated using the bulk and total intrusion (pore) volumes thus:

$$\phi = \frac{V_{\text{pore}}}{V_{\text{bulk}}}, \quad (2)$$

where V_{pore} is the total intrusion volume, (m^3) and V_{bulk} is the volume of the penetrometer minus volume of mercury in the penetrometer, measured at the end of the low pressure mercury injection, i.e.

$$V_{\text{bulk}} = V_{\text{penetrometer}} - \frac{\Delta w}{\rho_{\text{Hg}}}, \quad (3)$$

where Δw is the difference in weight of the penetrometer with sample at the end of the low pressure mercury injection minus penetrometer with sample under vacuum and ρ_{Hg} is the density of mercury (kg/m^3)

The permeability (in mD) calculation from the mercury injection is based on the power law approximation of Swanson (1966). Swanson showed that by drawing a line at 45° , tangent to the hyperbolic plot between mercury saturation and the capillary pressure, the portion of the sample effectively contributing to fluid flow can be determined. The permeability is then estimated thus:

$$\kappa = 399 \left[\frac{S_{\text{Hg}}}{P_c} \right]_A^{1.691}, \quad (4)$$

where P_c is the capillary pressure, (Pa); S_{Hg} is the mercury saturation, (% of bulk volume); A is the maximum value of S_{Hg}/P_c derived from the intersection between the 45° line and the hyperbolic plot.

Pore-size determination using the concept of most frequent pore

At every mercury injection pressure, the variations in saturation within the pore-space corresponding to certain radii r , is a variable fraction of the pore volume representing a percentage of the entire porous media. The peak of the curve corresponds to a certain pore-radius called “the most frequent pore” (e.g. Monicard 1980). Mercury intrusion is based on the capillary law governing liquid invasion into small pores.

Capillary forces in the reservoir are functions of surface and interfacial tensions, pore-size and shape and rock wettability. This law, in the case of a non-wetting liquid like mercury and assuming cylindrical pores is expressed by the (e.g. Washburn 1921) equation:

$$P_c = P_{Hg} - P_{air} = \frac{2\sigma_{Hg-air} \cos \theta_{Hg-air}}{r}, \tag{5}$$

where P_c is the capillary pressure, σ is the surface tension interfacial tension between mercury and air in dynes/cm (typically 480 dynes/cm), r is the pore-size (μm) and $\theta_{\text{Hg-air}}$ is the contact angle between mercury and air in degrees (typically 140°).

Equation 5 can convert a measured function $\alpha(P_c)$ into an equivalent function $\alpha(r)$ curve which is a cumulative pore-size distribution (PSD); indicating the combined pore volume with opening radius less than r . Basically, the pore-size distribution (PSD) is then simply the derivative (e.g. Leij et al. 2002):

$$f(r) = \frac{d\alpha(P_c)}{dr} \tag{6}$$

Experimental set-up, techniques and procedures

Formation geological background

Data set investigated comprised of seven whole core plug samples, representing two Arabian fields; *Khuff* and *Wasia* formations. *Khuff* is a massive interbedded limestone, dolomite and dolomitic limestone, with occasional anhydrite found in southern Ghawar Field, Eastern Saudi Arabia. The geologic age of the formation sampled ranges from Permian to Triassic. Laboratory experiments were conducted on five (5) carbonate samples obtained from Duhaysan which is a member of the *Khuff* formation (Dukhayyil and Tawil 2006).

The sandstone core samples were obtained from the *Wasia* formation. Lithologically, the middle cretaceous *Wasia* formation in the area can be divided into two major units: the Lower *Wasia* sequence of mainly siliciclastic

facies (Khafji, Safaniya, Mauddud and Wara Members) of Albian-early Cenomanian age and the Upper *Wasia* fine-grained siliciclastic and carbonate sequence (Ahmadi, Rumaila and Mishrif Members) of Cenomanian–Turonian age. The sample member investigated is the *Khafji* which is of middle cretaceous age. It is composed of sandstone and siltstone. A detailed description of the sedimentary facies in the *Wasia* members and their inter-relationships in terms of depositional environment can be found in Sharief et al. (1989).

Experimental set-up

Table 1 shows the description and measurements of the seven samples before the tests. The letters V and H are used to differentiate samples cut vertically through the parent rock from those obtained horizontally. The essence of obtaining samples in vertical and horizontal alignment is to investigate the effect of bedding strata on flow characteristics within the pore space. The core samples have been numbered 1–7 for easy identification.

Each core sample was prepared by first drilling out 3.81 cm diameter core both vertically and horizontally to the parent rock (Fig. 1). The samples are then cut into smaller pieces of $1.27 \times 1.27 \times 0.51$ cm sizes (Fig. 2) using core cutting machine. These smaller pieces allow the cores to fit into the penetrometer cup (see “Experimental procedure”) with enough clearance round the whole surfaces to enable the mercury to intrude the pores.

Experimental technique

An automatic pore intrusion (Fig. 3) combines an advanced pressure transducer system with a high-resolution analog-to-digital converter and specialised equilibration and measurement routines for data collection (Poston et al. 2011). The penetrometer (Fig. 4) is made of a sample cup bonded to a metal-clad, precision-bore and glass capillary stem. The choice of a penetrometer for the test is dependent

Table 1 Core sample data

Sample name	Core number	Sample weight (g)	Sample + penetrometer weight (g)	Assembly weight (g)
Duhaysan V	1	4.58	65.84	133.95
Duhaysan H	2	4.68	65.95	133.53
QT18 V	3	3.57	64.82	136.75
QT18 H	4	5.39	66.64	130.46
QT19 V	5	12.26	79.62	238.1
Khafji V	6	3.99	65.23	131.46
Khafji H	7	3.18	64.49	136.27

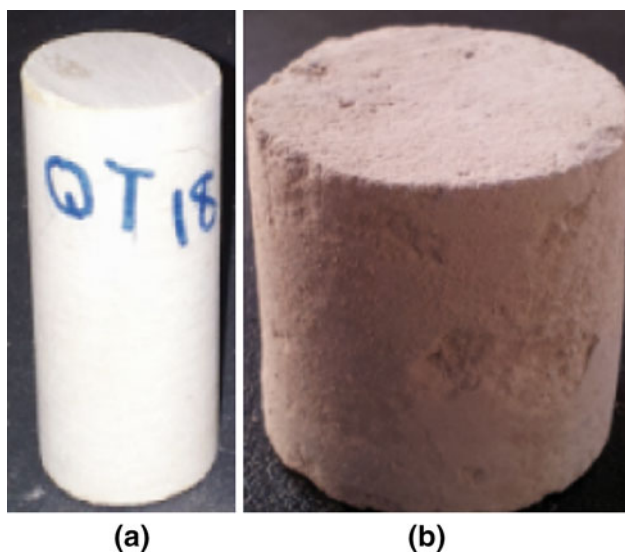


Fig. 1 Typical core samples from **a** sandstone and **b** carbonate Arabian formations

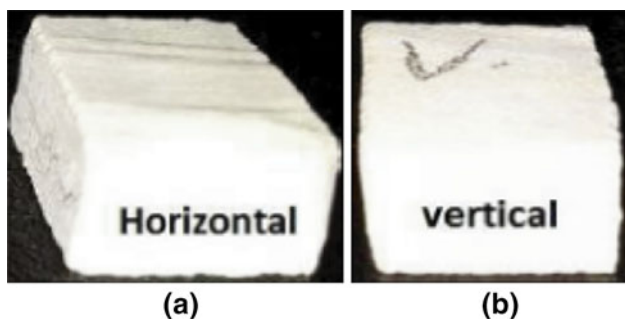


Fig. 2 Core samples cut into cuboidal shapes to allow placement into the penetrometer. **a** Horizontally and **b** vertically obtained core samples



Fig. 3 Micro-Meritics automatic mercury intrusion apparatus (Auto-Pore IV)

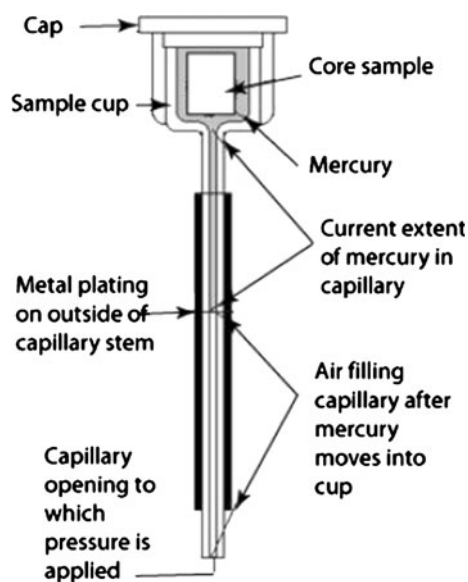


Fig. 4 Cross-section of a penetrometer in which pressure has forced some mercury into the pores of the sample and about 50 % of the stem capacity has been used (Modified from Dsouza and More 2008). Stem volumes of penetrometer used ranges from 0.392 to 1.131 mL

upon the sample volume and porosity. A valid test will normally require evacuation to remove contaminant gases and vapours (usually water) and also ensuring that not less than 20 % of the penetrometer stem volume is displaced into the sample (Dsouza and More 2008).

Experimental procedure

The core samples are first cleaned by extracting reservoir oil contained in it using a Soxhlet apparatus (Fig. 5). This is achieved by dripping a solvent usually toluene or a mixture of acetone and chloroform, over the core samples. In this method, the water and solvent are vapourised, recondensed in a cooled tube in the top of the apparatus and the water collected in a calibrated chamber (Soxhlet 1879). The solvent overflows and drips back over the samples. The oil removed from the samples remains in solution in the solvent. The duration of the cleaning process varies between 1 week for the carbonate, and 3 weeks for the sandstone core samples. The core samples are then dried in oven in readiness for the mercury intrusion experiment.

Mercury injection procedure

The mercury injection procedure can be described as follows:

1. The core sample is placed in the penetrometer and loaded in the low-pressure chamber of the equipment. The penetrometer is evacuated to a pressure of less than 20 μm of mercury, and then filled with mercury at



Fig. 5 Soxhlet apparatus containing some of the core samples used in this work

a pressure of 0.01 MPa (1.5 psia). The volume of mercury entering the larger pores in the core sample is monitored. During this stage, pores of diameters down to about 0.36 mm are filled.

- Mercury is injected incrementally into the core sample from 0.01 MPa (1.5 psia) to 0.2 MPa (30 psia), using nitrogen gas as the displacing medium. At each pressure increment, mercury intrusion is monitored while the pressure is held constant. Equilibrium is reached when the intrusion rate drops below 0.001 $\mu\text{L/g/s}$. The pressure and the total volume for each point are recorded.
- The low-pressure stage is complete at the end of the 0.2 MPa (30 psia) injection. The pressure is then reduced to atmospheric and the penetrometer together with the mercury intruded sample removed and weighed (the assembly weight).
- The sample is then loaded into the high-pressure chamber of the equipment and mercury injected incrementally from 0.2 MPa (30 psia) to 414 MPa (60,000 psia), using hydraulic oil as the displacing medium.
- The test is complete when the high pressure stage of 414 MPa (60,000 psia) is reached and the injection pressure is reduced to atmospheric. During this stage, pores down to about 0.003 μm are filled.

The volume of mercury injected at each pressure determines the non-wetting (i.e., mercury) saturation, S_{Hg} . The equilibration time for the low and high pressure cells are generally 20 and 45 s, respectively. In the equilibration mode, an accurate measurement of pressure is achieved with the high-resolution system. These data provide the basis for the calculation of pore volume, pore area, pore

distribution and sample density. The assigned operating conditions can be stored as a template and reassigned to other samples, thereby saving time and minimising the potential for human error.

Results and discussion

The capillary pressure versus mercury saturation ($P_c - S_{\text{Hg}}$) plots for all the samples are shown in Figs. 6, 8 and 10 while the pore-size distribution for all the core samples studied are shown in Figs. 7, 9 and 11. The $P_c - S_{\text{Hg}}$ and pore-size distribution plots for the cores 3 and 5 are similar; hence only 3 is shown.

As can be seen in Figs. 6, 8 and 10, the capillary pressure required for the mercury to intrude the pore-space, is strongly dependent on pore-size distribution (Figs. 7, 9 and 11). The entry pressures (P_{entry}) were observed to be consistently high for all the carbonate core samples obtained vertically as opposed to those obtained horizontally. The sandstone have relatively smaller entry pressure (P_{entry}) with the pore-size distribution well shifted to the right. The estimated permeability–porosity ($\kappa - \phi$) relationship for the five (5) tight carbonate samples and two (2) sandstone samples is displayed in Fig. 12.

The root mean square error (RMSE) between the predicted and actual intrusion volumes; $V_{\text{predicted}}$ and V_{actual} , respectively, over n pressure data points for each of the core samples is calculated thus:

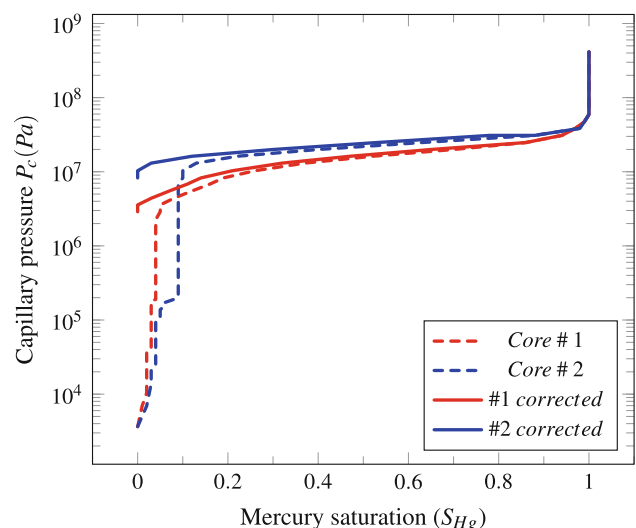


Fig. 6 Plots of capillary pressure versus mercury saturation for the carbonate core samples 1 and 2. The red and blue colours represent vertically and horizontally obtained samples, respectively. The dash and thick lines represent the uncorrected and conformance corrected data, respectively

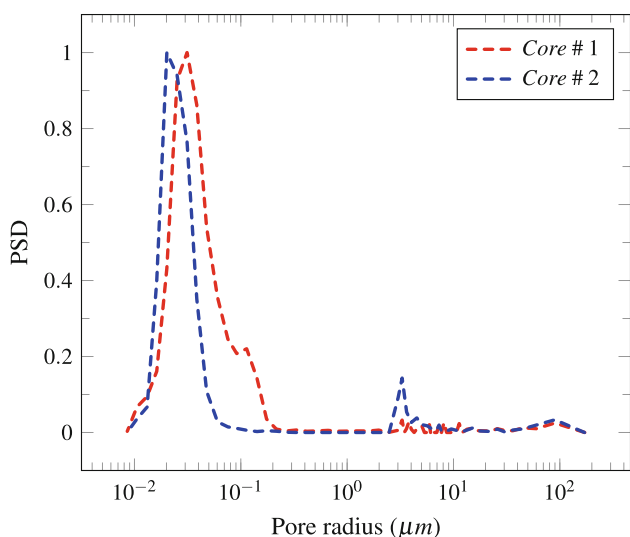


Fig. 7 Normalised pore-size distribution (PSD) for samples 1 and 2

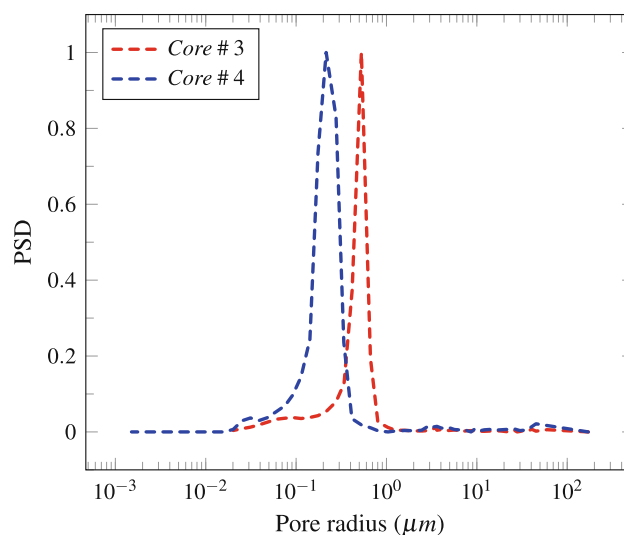


Fig. 9 Normalised pore-size distribution (PSD) for samples 3 and 4

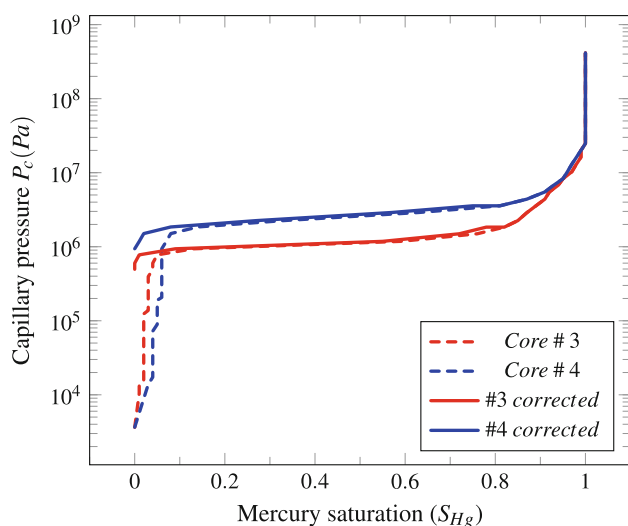


Fig. 8 Plots of capillary pressure versus mercury saturation for the carbonate core samples 3 and 4. The red and blue colours represent vertically and horizontally obtained samples, respectively. The dash and thick lines represent the uncorrected and conformance corrected data, respectively

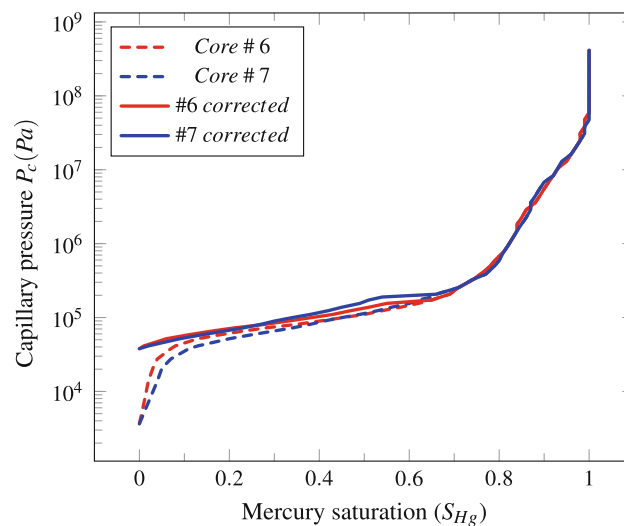


Fig. 10 Plots of capillary pressure versus mercury saturation for the carbonate core samples 6 and 7. The red and blue colours represent vertically and horizontally obtained samples, respectively. The dash and thick lines represent the uncorrected and conformance corrected data, respectively

$$\text{RMSE} = \sqrt{\frac{\sum_{i=1}^n (V_{\text{predicted}} - V_{\text{actual}})^2}{n}}, \quad (7)$$

and the pore fractal dimension which quantifies the fractal geometry of the core sample is estimated (see Webb 2001). Table 2 shows the root mean square (RMSE) and the fractal dimension of the core samples investigated. The volumetric RMSE are generally low for all the samples and 0 for the sample QT19 V with a fractal dimension of 3.

It is known that the accuracy of the mercury injection experiment particularly for tight samples, is dependent on the degree of sample roughness (or external irregularity)

and must be removed from the capillary pressure curve before an estimate of permeability is attempted. This is known as conformance correction and always occurs in the low pressure portion of the injection profile. Therefore, a systematic approach similar to that suggested by Comisky et al. (2007) was employed in the conformance correction of all the samples. In all the capillary pressure curves (Figs. 6, 8, 10), the dash curves represent the uncorrected injection profile while the thick curves are the conformance corrected injection profile.

Further, in the high pressure region, the capillary pressure should be corrected for the effect of material

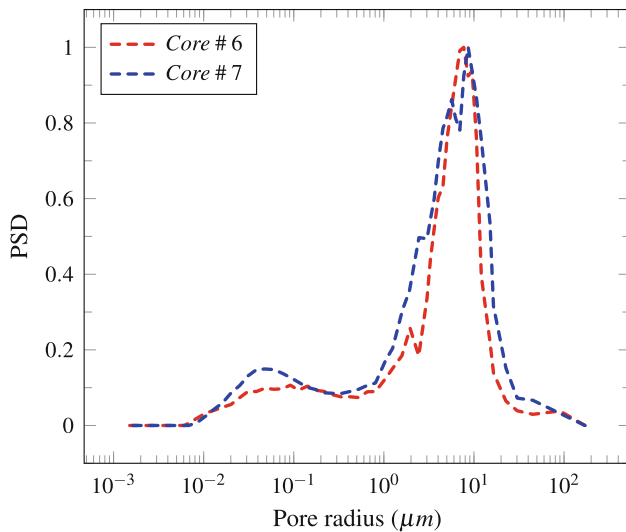


Fig. 11 Normalised pore-size distribution (PSD) for samples 6 and 7

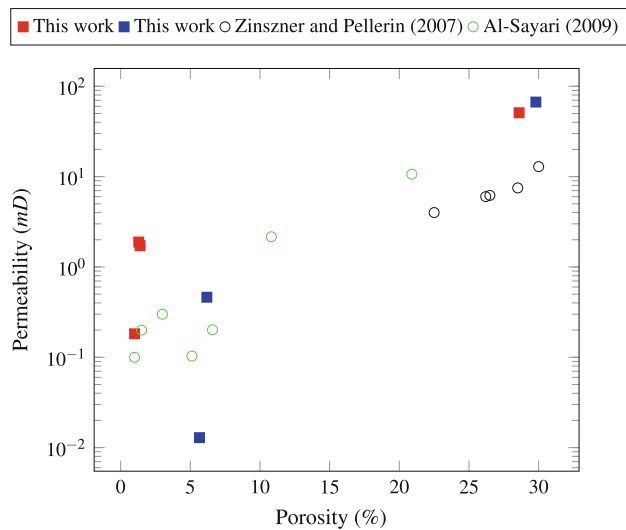


Fig. 12 Plots of permeability versus porosity for all the measured samples and some selected published data (Zinszner and Pellerin 2007; Al-Sayari 2009)

compression, void collapse or both. Although, this correction, known as the 'blank' correction tends to have little effect on the estimated permeability due to the fact that most of the permeability models use the low pressure region of the capillary pressure curve; it can lead to the deviation of the data from expected asymptotic trend (see for instance Webb 2001). The penetrometers used in this work were all calibrated with a set of 'blank' runs made with plugs of varying sizes to give a blank corrected capillary pressure data.

As can be seen in Figs. 7, 9 and 11, the average pore-size is consistently higher for the cases where the cores were obtained vertically from the parent rock compared to those obtained horizontally. The corresponding high permeability measured in these samples (Fig. 12) suggests that these large pores are well connected and therefore contribute largely to flow (Table 3).

The pore-size distribution is well known to strongly affect the permeability (e.g. Bear 1988; Dullien 1979; Garcia et al. 2009; Zinszner and Pellerin 2007) and this is also observed in our experiments. Also, given that the main factors affecting the absolute permeability are length-scales associated with the grain-size in the first place and secondly the porosity (e.g. Garcia et al. 2009), published experimental data in the low porosity range of carbonate samples from Zinszner and Pellerin (2007) were selected for comparison purposes. The $\kappa - \phi$ for the carbonate samples investigated in this work, compares very well with the experimental data of Zinszner and Pellerin (2007) (Fig. 12). Our technique, however, permits the characterisation of sensitive core samples from carbonate formations with permeability much less than 1 mD. The permeabilities of core samples obtained vertically from the parent rock were up to two orders of magnitude greater than those measured from cores obtained horizontally. Figure 12 also contains selected Arabian sandstone data from Al-Sayari 2009 in which the permeability of the core samples were measured using mercury injection approach. Within the same porosity range, our data are about five times higher

Table 2 Root mean square error (RMSE)

Sample name	Sample weight (g)	RMS error (cm ³ /g)	RMS error (cm ³)	Fractal dimension
Duhaysan V	4.58	0.00106	0.00487	2.702
Duhaysan H	4.68	0.00265	0.01241	2.198
QT18V	3.57	5.547E-05	0.00020	2.996
QT18 H	5.39	4.474E-05	0.00024	2.993
QT19 V	12.26	0	0	3.0
Khafji V	3.99	0.00018	0.00071	2.972
Khafji H	3.18	0.00029	0.00093	2.973

Table 3 Summary of measured data

Core sample	Porosity (ϕ , %)	Formation factor	Permeability (κ , mD)	Tortuosity τ	Entry pressure (psia)
1	1.0	0	7.44	10.26	418
2	6.2	0.002	0.46	47.86	1,196
3	1.2	0.031	0.18	78.25	72
4	5.7	0.009	0.01	208.3	136
5	1.25	0.007	1.72	16.04	20
6	28.6	0.025	50.9	9.95	5.4
7	29.8	0.017	66.9	8.56	5.4

than their reported data; which is very good, given that permeability can range by several orders of magnitude in the same geological formation.

In order to further understand the effects of low porosity and low permeability on the flow behaviour in the tight carbonate samples, the tortuosity τ and formation resistivity measured experimentally were analysed. Comparing samples 1, 3, 5 and 6, 7 shown in Table 3, it can be seen that the tortuosity and formation resistivity factor decrease as the permeability increases at relatively constant porosity. This trend exhibited by the rock-pore characteristics investigated in this work is comparable to the published trends of τ and porosity ϕ in the literature (Amyx et al. 1960; Owolabi and Watson 1993; Pape et al. 1998).

Conclusion

A high-pressure automatic mercury injection apparatus was used to derive basic routine core data governing flow in tight formations. The entry capillary pressures in the carbonate samples which have very low permeability, were observed to be much higher than the fairly homogeneous clastic core samples by up to three orders of magnitude. Also, the permeabilities of core samples obtained vertically from the parent rock were up to two orders of magnitude greater than those measured from cores obtained horizontally.

Although, our technique already considered the conformance correction as suggested by previous authors (e.g. Comisky et al. 2007); it is clear that additional work is required in characterising and improving the precision of methods for estimating permeability of tight cores using mercury injection tests. Further analysis of core images under high resolution in both lateral and vertical coordinates, could also improve our understanding of flow behaviour in tight formations.

Acknowledgments The authors acknowledge the members of the Oil and Gas Research Institute at King Abdul Aziz Center for Science and Technology (KACST), Riyadh Saudi Arabia, for their supports in carrying out this research. We are also grateful to the members of staff and Al-Amoudi chair at the Petroleum and Natural Gas Engineering Department, King Saud University for providing us with the sandstone core samples used in this work.

Open Access This article is distributed under the terms of the Creative Commons Attribution License which permits any use, distribution, and reproduction in any medium, provided the original author(s) and the source are credited.

References

- Akanji LT, Matthai SK (2010) Finite element-based characterization of pore-scale geometry and its impact on fluid flow. *Transp Porous Media* 81:241–259
- Al-Sayari S (2009) The influence of wettability and carbon dioxide injection on hydrocarbon recovery. PhD thesis, Department of Earth Science and Engineering, Imperial College London
- Amyx JW, Bass DM, Whiting RL (1960) Petroleum reservoir engineering. McGraw-Hill Book Co., New York
- Archie GE (1950) Introduction to petrophysics of reservoir rocks. *AAPG Bull* 34:943–961
- Bahrami H, Rezaee R, Ostojic J, Nazhat D, Clennell B (2011) Evaluation of damage mechanisms and skin factor in tight reservoirs. In: *SPE*, 142284, pp 1–13
- Bear J (1988) Dynamics of fluids in porous media. Dover INC, New York
- Bliefnick DM, Kaldi JG (1996) Pore geometry; control on reservoir properties, walker creek field, columbia and lafayette counties, arkansas. *Am Assoc Petroleum Geol Bull* 80:1027–1044
- Brooks RH, Corey AT (1981) A simple correlation between permeability and mercury capillary pressures. *J Petroleum Technol* 3:2488–2504
- Comisky JT, Newsham KE, Rushing JA, Blasingame TA (2007) A comparative study of capillary-pressure-based empirical models for estimating absolute permeability in tight gas sands. In: *SPE*, 110050, p 18
- Dastidar R, Sondergeld CH, Rai CS (2007) An improved empirical permeability estimator from mercury injection for tight clastic rocks. *Petrophysics* 48(3):186–187
- Dsouza J, More HN (2008) Mercury intrusion porosimetry: a tool for pharmaceutical particle characterization. *Pharm Inf* 6(2):1–10. Available at: <http://www.pharmainfo.net/reviews/mercury-intrusion-porosimetry-tool-pharmaceutical-particle-characterization>. Accessed 23 July 2012
- Dukhayil RKA, Tawil AAA (2006) Reservoir architecture of the triassic khartam carbonate sequence, khuff outcrop analogue in al-qassim, central saudi arabia. In: *GEO Middle East Conference and Exhibition*, p 1
- Dullien F (1979) Porous media: Transport and microstructure, 2nd edn. Academic Press, New York
- Garcia X, Akanji LT, Blunt MJ, Matthai SK, Latham JP (2009) Numerical study of the effects of particle shape and polydispersity on the single-phase permeability. *Phys Rev E* 80:1539–3755
- Huet CC, Rushing JA, Newsham KE, Blasingame TA (2005) A modified purcell/burdine model for estimating absolute permeability from mercury injection capillary pressure data. In: *International Technology Conference, Doha*, no. 10994 in 2118, p 21
- Katz AJ, Thompson AH (1981) Quantitative prediction of permeability in porous rock. *Phys Rev B* 34(11):8179–8181
- Katz AJ, Thompson AH (1987) Prediction of rock electrical conductivity from mercury injection measurements. *J Geophys Res* 92(B1):599–607
- Khan AA, Rehman SA, Akram AH, Ahmad A (2011) Factors affecting production behaviour in tight gas reservoirs. In: *SPE*, no. 149045 in 2118, p 21
- Klinkenberg LJ (1941) The permeability of porous media to liquids and gases. In: *API Drilling and Production Practice paper presented at the API 11th Mid-Year Meeting, Tulsa, OK*, pp 200–213
- Leij FJ, Ghezzehei TA, Or D (2002) Modeling the dynamics of the soil pore-size distribution. *Soil & Tillage Reseach* 64:61–78
- Melas FF, Friedman GM (1992) Petrophysical characteristics of the jurassic smackover formation, jay field. *Am Assoc Petroleum Geol Bull* 76:81–100
- Melrose JC, Dixon JR, Mallinson JE (1994) Comparison of different techniques for obtaining capillary pressure data in the low-saturation region. In: *Annual Technical Conference and Exhibition, Dallas, Texas, SPE*, pp 185–192
- Monicard RP (1980) Properties of Reservoir Rocks: Core Analysis. Gulf Publishing Company, Houston

- Owolabi OO, Watson RW (1993) The influence of porosity, permeability, tortuosity, wettability and mercury porosimetry properties on limestone waterflood residual oil saturation. In: SCA Conference, SCA, 9309, p 16
- Pape H, Clauser C, Iffland J (1998) Permeability prediction for reservoir sandstones and basement rocks based on fractal pore space geometry. In: SEG, pp 1447–1460
- Pittman ED (1992) Relationship of porosity and permeability to various parameters derived from mercury injection- capillary pressure curves for sandstone. AAPG Bull 76(2):191–198
- Poston M, Dudu L, Thornton T, Bouza P, Thiele G, Brown R (2011) Effects of particle shape on measured particle size. In: Micromeritics, micromeritics, p 1
- Purcell WR (1949) Capillary pressures-their measurement using mercury and the calculation of permeability. Trans AIME 186:39–48
- Sharief FA, Magara K, Abdulla HM (1989) Depositional system and reservoir potential of the middle cretaceous wasia formation in central-eastern arabia. Marine Petroleum Geol 6:303–315
- Soxhlet F (1879) Die gewichtsanalytische bestimmung des milchfettes. Polytechnisches J (Dingler's) 232:461–465
- Swanson BF (1966) Properties of porous media affecting fluid flow. J Irrigation Drainage Eng 92:61–88
- Thompson AH, Katz AJ, Raschke RA (1987) Prediction of rock electrical estimation of absolute permeability from capillary pressure measurements. In: Annual technical conference and exhibition, 16794, pp 599–607
- Vavra CL, Kaldi JG, Sneider RM (1992) Geological applications of capillary pressure: A review. Am Assoc Petroleum Geol Bull 76:840–850
- Walls JD, Amaefule JO (1985) Capillary pressure and permeability relationships in tight gas sands. In: SPE Low Permeability Gas Reservoir Denver, CO, 13879, pp 186–187
- Washburn EW (1921) The dynamics of capillary flow. Phys Rev 17(3):273
- Webb PA (2001) An introduction to the physical characterization of materials by mercury intrusion porosimetry with emphasis on reduction and presentation of experimental data. MicroMeritics Instrument Corp, Norcross, Georgia. Available at: http://www.particletesting.com/docs/intro_mip.pdf. Accessed 12 Mar 2013
- Zinszner B, Pellerin FM (2007) A Geoscientist's Guide to Petrophysics. IFP Publications, Paris